



Encapsulation of Ginger Essential Oil Using Complex Coacervation Method: Coacervate Formation, Rheological Property, and Physicochemical Characterization

Lolene Tavares¹ · Cacioano Pelayo Zapata Noreña¹

Received: 19 March 2019 / Accepted: 17 June 2020 / Published online: 26 June 2020
© Springer Science+Business Media, LLC, part of Springer Nature 2020

Abstract

Ginger essential oil (GO) was encapsulated with whey protein isolate (WPI)/gum Arabic (GA) and GA/chitosan (CH) complex coacervates. Best complex coacervate yields (43 and 73%) were obtained when using mass ratios of 3:1 (w:w), for WPI/GA, and of 5:1 (w/w) for GA/CH, respectively, and both behaved as shear thinning fluids. Frequency sweep revealed that G'' predominated over G' for the both complex coacervate at low frequency values, and a crossover between the viscoelastic moduli occurred at about 5 Hz for GA/CH and at 60 Hz for WPI/GA. The magnitude of the viscoelastic moduli was higher for GA/CH than for WPI/GA. The creep-recovery tests showed that the coacervates with GO resulted in higher compliance values and weaker internal network structures. The Burgers model equation and exponential decay function were adequate to adjust the experimental data and describe the coacervate creep and recovery behavior, respectively. The obtained coacervates were freeze-dried for 48 h and then characterized concerning entrapment efficiency, Fourier transform infrared (FTIR), scanning electron microscopy (SEM), thermogravimetric analysis (TGA), solubility, and hygroscopicity. FTIR analyses revealed that only physical interactions occurred between the functional groups of GO and of WPI/GA and GA/CH complexes. TGA showed that wall materials contributed to a significant increase in the GO thermal stability and also evidenced some non-encapsulated GO present on the surface of WPI/GO/GA powders. The entrapment efficiency was 55.31 and 81.98% using complex of GA/CH and WPI/GA, respectively, revealing GA/CH as a more efficient complex for the GO protection ($p < 0.05$).

Keywords Ginger essential oil · Encapsulation · Whey protein isolate · Chitosan · Gum Arabic · Complex coacervation

Introduction

Ginger has been widely cultivated mostly in tropical countries, such as Australia, Brazil, China, Japan, Mexico, West Africa, West Indies, and parts of the USA (Ukeh et al. 2009). Their rhizomes are mainly used as flavoring food, dietary supplement, and in medicine since antiquity (Srinivasan 2017) and contains 60–70% carbohydrates, 3–8% crude fiber, 9% protein, 8% ash, 3–6% fatty oil, and 2–3% of essential oil (Jakribettu et al. 2016). The ginger essential oil is composed of sesquiterpene (α -zingiberene) (30–70%), β -sesquiphellandrene (15–20%), β -bisabolene (10–15%), α -

farnesene, and some monoterpenoids (β -phellandrene, camphene, and cineol) (Srinivasan 2017). The constituents of ginger essential oil and their proportion depend on the genetic characteristics, soil composition, weather conditions, and the analytical method used (Wang et al. 2017). Ginger essential oil has antimicrobial, antifungal, and antioxidant activities, being used for the treatment of various diseases and disorders (Singh et al. 2008; Bellik 2014; Stoyanova et al. 2006). However, ginger essential oil is unstable and susceptible to oxidation and degradation in the presence of oxygen, light, metals, and high temperature (Fernandes et al. 2016a, b). Microencapsulation is a process widely used in the protection of heat-sensitive compounds such as essential oil. In this process, essential oil compounds are entrapped within the wall materials, enhancing their protection against oxidation and volatilization, broadening its application range in food products, and improving cost-effectiveness for the food manufacturer. In addition, it allows a controlled essential oil release, facilitating handling, storage, and increasing shelf life without

✉ Cacioano Pelayo Zapata Noreña
czapatan@ufrgs.br

¹ Institute of Food Science and Technology, Federal University of Rio Grande do Sul, Av. Bento Gonçalves, No. 9500, Porto Alegre, RS CEP 91501-970, Brazil

changing the original food properties (Ye et al. 2018; Castro-Rosas et al. 2017). Microencapsulation by complex coacervation has been used in a wide range of applications (Comunian et al. 2013). Complex coacervation results from the electrostatic interactions of oppositely charged biopolymers in an aqueous medium, leading to separation into two phases, a dense coacervate phase rich in polymer and the other liquid phase depleted in polymers (Eghbal and Choudhary 2018; Ezhilarasi et al. 2013). Complex coacervate process is affected by many factors such as pH, concentration, medium ionic strength, biopolymers ratio, temperature, and agitation time (Timilsena et al. 2019).

Whey protein isolate (WPI) is a globular and soluble protein obtained as a secondary product derived from cheese and casein manufacture industries, representing about 20% of the milk proteins (Kilara and Vaghela 2018). WPI, with a minimum of 90% protein content, is widely used as wall material due to its physicochemical and functional properties and capacity to stabilize oil-in-water emulsion systems (Stang et al. 1994; Touré et al. 2011; Fan et al. 2017; Eratte et al. 2017). Gum Arabic is a natural polysaccharide exuded by *Acacia* sp. trees (Shi et al. 2017) and has been used as wall material for microencapsulating essential ginger oil, as it is considered an effective emulsifying agent and for providing protection against oxidation (Wu et al. 2018; Fernandes et al. 2016b). Chitosan is a cationic polysaccharide obtained by deacetylation of chitin. Structurally, it is composed of d-glucosamine and N-acetyl-d-glucosamine units, linked by β -1,4 glycosidic linkages (Muxika et al. 2017). Chitosan is a polymer with a wide variety of applications because of its biodegradable, biocompatible, non-toxicity, and functional properties such as antimicrobial, anticoagulant, antioxidant, analgesic, and cholesterol lowering (Ngo et al. 2015; Muxika et al. 2017).

There are several works reporting the spray-drying microencapsulation of ginger essential oil (de Barros Fernandes et al. 2017; Fernandes et al. 2016a, b; Touré et al. 2011), but none about its microencapsulation with complex coacervates. Although WPI/GA and GA/CH complex coacervates have been used for encapsulating different functional compounds (Eratte et al. 2017; Eratte et al. 2014; Eratte et al. 2015; Tan et al. 2016; Butstraen and Salaün 2014), they have not been used for encapsulating GO. In addition, this study presents a novel approach to describe the viscoelasticity of the coacervates, prepared before drying, in terms of creep and recovery behavior and aims to explain the relationship between viscoelastic properties determined by dynamic and static tests.

The objectives of this work were to establish the conditions leading to the best complex coacervate yield between WPI/gum Arabic (GA) and GA/chitosan (CH), to microencapsulate ginger essential oil (GO) in both complex coacervate matrices, to characterize several physicochemical characteristics of the complex coacervates and of the ginger oil microencapsulates,

including flow, static and dynamic rheological properties, thermogravimetric analysis (TGA), Fourier transform infrared (FTIR) spectroscopy, morphology, solubility, and entrapment efficiency.

Materials and Methods

Materials

Fresh ginger oil (*Zingiberis Rhizoma* L.) was acquired from Ferquima (São Paulo, Brazil). WPI with a protein content of 92% was kindly donated by Arla Foods Ingredients (São Paulo, Brazil). Chitosan with degree of deacetylation (DD) of 96% was kindly donated by Primex (Siglufjördur, Iceland) and gum Arabic (Instantgum BA) from *Acacia senegal* trees was purchased from Nexira (São Paulo, Brazil). Sodium hydroxide (NaOH), hydrochloric acid (HCl), and acetic acid both with analytical grade were purchased from Sigma-Aldrich.

Preliminary Assays of Complex Coacervation Optimization

Zeta Potential Profile

The pH of each biopolymer dispersion and the final charge after a mixture of biopolymers affect the attraction and consequent complexation between them (Chang et al. 2016). Therefore, the electrical charge (zeta (ζ)-potentials) of each biopolymer dispersions of GA, CH, and WPI, all prepared at 1% (w/w), were determined using a ZetaPALS equipment (Brookhaven Instruments, 31450). The CH 1% (w/w) was prepared dissolving the correspondent powder in acetic acid solution 0.1% (volume/volume (v/v)). The GA and WPI (1%, w/w) solutions were prepared in deionized water. Each biopolymer solution was mixed by magnetic stirring (Fisaton, model 752A) for 30 min. The aqueous solutions of 0.1 and 1 M for both HCl and NaOH were used for pH adjustment in the range from 2 to 6 using a pH meter (Quimis, Model Q-400M1). Each sample was put into a ζ -potential cell and measurements were conducted in triplicate at 20 °C.

Determination of Coacervate Yield

The mixing ratio of biopolymers is an important factor in the complex coacervation process (Chang et al. 2016). In this sense, the effects of WPI/GA and GA/CH ratios on the formation of complex coacervation were evaluated by coacervate yield. The coacervates were obtained by the mixing method, which consists in preparing the biopolymer dispersions separately and adjusting their pH to the optimal interaction pH, in order to promote rapid electrostatic interaction between the

biopolymers (Turgeon and Laneville 2009). The optimum pH used to obtain the maximum WPI/GA and GA/CH complex coacervates were fixed in pH 3.75 and 3.6, respectively, according to studies realized by Eratte et al. (2014) and Butstraen and Salaün (2014), respectively. In the WPI/GA complex coacervate, the WPI 3% (w/w) and GA 3% (w/w) dispersions were prepared separately in deionized water. Each dispersion was mixed in a magnetic stirrer, at 300 rpm, for 2 h, and HCl solution (1 M) was used to adjust the pH for 3.75. For the GA/CH complex coacervate, the GA 3% (w/w) was prepared separately in deionized water and CH 3% (w/w) was prepared in 2% acetic acid solution. Each dispersion was stirred at 300 rpm for 2 h and HCl solution (1 M) was used to adjust the pH to 3.6. Then, all the dispersions were allowed to rest for 24 h to a complete hydration. After that, for complex coacervation of WPI/GA, the WPI 3% (w/w) dispersions were mixed with GA 3% (w/w) dispersions at different mass ratios of 1:1, 2:1, 3:1, 4:1, 5:1, 6:1, and 7:1 (w/w). For GA/CH, the GA 3% (w/w) dispersions were mixed with CH 3% (w/w) dispersions at the same mass ratios reported above.

All the complex mixtures were mixed in the magnetic stirrer for 30 min and then allowed to stabilize for 5 h at 20 °C. The supernatants were discarded and the precipitated coacervates were dried in an oven (Biomatic, model 303) at 105 °C for 24 h. The coacervate yield was calculated according to Eq. 1:

$$CY = \frac{w_d}{w_t} \times 100 \quad (1)$$

where CY is the yield of complex coacervates (%), w_d is the weight of dried coacervates, and w_t is the total weight of both biopolymers utilized in the mixture formations.

Microencapsulation Process

Complex Coacervation Systems

The GO emulsion was prepared according to the method described by Fernandes et al. (2016b), with some modifications. The mass ratio between the GO and biopolymers used in each encapsulation process was set at 1:3 (w/w). In order to study two systems of encapsulation, the GO was slowly added into each dispersions of GA 3% (w/w) previously prepared at pH 3.60 and 3.75. Then, the emulsion was homogenized using a high-speed homogenizer (Ultra-Turrax IKA, T18) at 4000 rpm for 5 min. The resultant emulsion was submitted to ultrasonication (Branson Digital Sonifier®, S-450D) at 160 W, 20 kHz for 2 min. After that, the solution of WPI 3% (w/w) at pH 3.75 was slowly added into the emulsion of GA/GO at pH 3.75 and the solution of CH 3% (w/w) in the emulsion of GA/GO at pH 3.60, according to coacervate yield. Then, the resultant mixture was stirred with a magnetic stirrer for 30 min and allowed to stabilize for 5 h at 20 °C.

Finally, the supernatants were discarded and the precipitated phase was frozen in ultra-freezer (Liobras, Liotop UFR 30) at -80 °C for 24 h.

Freeze Drying

The frozen precipitated phase (coacervates with and without incorporation of GO) was dried in a freeze-dryer (Liobras, LIOTOP L101) at -57 °C at vacuum pressure less than 130 μ mHg. The samples were removed at specific time intervals (16 h) and weighed until reaching constant weigh (at the end of 48 h). Then, the samples were crushed using a mortar and pestle. The resultant microparticles were placed in polyethylene bags, sealed, and placed in aluminum pouches. The samples were stored in a desiccator containing silica for further analyses.

Rheological Measurements

The rheological properties were performed in the fresh coacervates (before freeze drying). The tests were performed in the coacervates with and without incorporation of GO using a modular rheometer (Thermo Scientific, Haake Mars 40/60), with a cone-plate geometry (diameter 35 mm, angle 2°). The viscosity of the samples was measured using a steady-state flow program varying shear rate from 0.1 to 100 s^{-1} . The viscoelastic properties were determined using two types of analyses: static (creep-recovery) and dynamic flow measurements. In the dynamic measurements, values of the storage modulus (G') and the loss modulus (G'') were registered in a frequency sweep test (from 0.1 to 100 Hz), with a constant strain (0.1 Pa) within the linear viscoelastic region (LVR).

Creep and recovery tests were performed applying a constant stress of 1 Pa, within the LVR, on the sample for 90 s and allowing strain recovery for the same time, after removal of the load. The results of the compliance function against time were expressed according to Eq. 2:

$$J_t = \frac{\gamma(t)}{\tau_0} \quad (2)$$

where τ_0 is the constant stress applied (Pa) and $\gamma(t)$ is a resulted strain time-dependent. The creep (J_C) (0 to 90 s) and recovery (J_R) (90 to 180 s) compliances of the coacervate structure behavior were described by the Burgers model (Eq. 3) (representing the Maxwell and Kelvin–Voigt models placed in series) and an exponential decay function (Eq. 4), respectively (Karaman et al. 2012; Augusto et al. 2013)

$$J_c = \frac{1}{G_0} + \frac{1}{G_1} \times \left[1 - \exp\left(\frac{-tG_1}{\eta_1}\right) + \frac{t}{\eta_0} \right] \quad (3)$$

where G_0 is the instantaneous shear modulus of the Maxwell unit, η_0 represents the residual viscosity (dashpot contribution)

of the Maxwell element, G_1 is the shear modulus of Kelvin–Voigt, and η_1 represents the internal viscosity (dashpot contribution) of Kelvin–Voigt unit.

$$J_R = J_\infty + J_{1R} \exp(-Bt^C) \quad (4)$$

where J_∞ and J_{1R} represent the recovery compliances of the Maxwell dashpot and Kelvin–Voigt element, respectively. B and C are parameters that define the recovery speed of the system.

The capacity of the sample to recovery was calculated according to Eq. 5, described by Dolz et al. (2008):

$$\%R = \frac{J_{\max} - J_\infty}{J_{\max}} \quad (5)$$

where $\%R$ is the total recovery percentage, J_{\max} represents the maximum compliance, and J_∞ is recovery compliance of the Maxwell dashpot.

Experimental data were fitted to the Burgers and exponential models. The parameters of the models were obtained using the Levenberg–Marquardt algorithm in the MATLAB® curve-fitting toolbox.

Characterization of the Microparticles Powders

Moisture Content

The moisture content of the microparticles was determined gravimetrically by oven-drying at 105 °C until reaching constant weight (AOAC 1990).

Hygroscopicity

The hygroscopicity was determined according to Cai and Corke (2000), with minor modifications. One gram of sample was placed in a container containing saturated NaCl solution (75% RH) and then stored in an incubator chamber (Ethik Technology, 411/FDP) at 25 °C for 1 week. After that, the samples were weighed every 24 h until equilibrium (no weight change) was achieved. The hygroscopicity was expressed as a gram of adsorbed moisture per 100 g dry solids (g/100 g).

Solubility

The solubility of freeze-dried powder was determined according to Cano-Chauca et al. (2005), with minor modifications. One gram of each sample was weighed and mixed with 100 mL of distilled water for 30 min using a magnetic stirrer. Then, the solution was centrifuged (Thermo Fisher Scientific, Heraeus Megafuge 16R) at 3000×g for 5 min. Twenty-five milliliters of the supernatant was transferred to a beaker and dried in an oven at 105 °C until constant weight. The solubility (%) was calculated by the weight difference.

Entrapment Efficiency

Entrapment efficiency (EE) corresponds to the percentage of GO present in the microparticles that were actually encapsulated (Rutz et al. 2017). Therefore, the total GO present in WPI/GO/GA and GA/GO/CH microparticles (C_t) were quantified by weighing 100 mg of microparticles, adding 10 mL of ethyl acetate for WPI/GO/GA and 10 mL of a mixture of ethyl acetate:water (1:1 v/v) for GA/GO/CH. Then, each dispersion was homogenized using a high-speed homogenizer (Ultra-Turrax IKA, T18) at 13,000 rpm for 1 min, followed by centrifugation at 3000g for 5 min (Rutz et al. 2017). Thus, the wall structure of the powders was completely destructed to release GO content present in microparticles. For the GA/GO/CH dispersions, due to the presence of polar and non-polar phases, the non-polar phase which contains GO was carefully separated from the aqueous phase. The recovered non-polar phase was transferred into 10-mL volumetric flasks and diluted to the mark with ethyl acetate.

The non-encapsulated GO present on the surface of the powders (C_s) was quantified by homogenizing 100 mg of sample with 10 mL of ethyl acetate in a vortex mixer for 1 min, followed by centrifugation at 1060g for 3 min. The resultant above supernatants were recovered and then transferred into 10-mL volumetric flasks and diluted to the mark with ethyl acetate. The amount of GO was quantified by measuring absorbance at 270 nm in a UV-vis spectrophotometer (Genesys S10, Thermo Scientific) (Fernandes et al. 2016b). The concentration of GO was calculated using a calibration curve, obtained by measuring absorbance of GO diluted with ethyl acetate at different known concentrations.

The entrapment efficiency was calculated according to Eq. 6:

$$EE\% = \frac{C_t - C_s}{C_t} \quad (6)$$

where C_t represents the total GO present in the microparticles and C_s is the non-encapsulated GO present on the surface of the powders.

Thermogravimetric Analysis

The thermal stability of microparticles was performed on a Pyris 1 TGA (PerkinElmer) thermal analyzer under a nitrogen atmosphere with a flow rate of 20 mL min⁻¹. The samples (approximately 10 mg) were placed in an aluminum crucible and then heated from 20 to 700 °C with a gradient of 20 °C min⁻¹.

Morphology

The structures and the surface morphologies of microparticles were analyzed by scanning electron microscopy (SEM). The

microparticles were adhered to SEM aluminum stubs using a double-sided adhesive carbon tape, coated with gold, and then examined by scanning electron microscope (JEOL, JSM-6060) with an accelerating voltage of 8 kV and magnification of $\times 300$.

Fourier Transform Infrared Spectroscopy

FTIR spectra of dried coacervates and bulk GO were obtained using an infrared spectrometer (Jasco, FTIR-410). Each dried coacervate sample was mixed with KBr (potassium bromide) and compressed into a disc using a hydraulic press. FTIR spectra were recorded in the range 4000 to 400 cm^{-1} .

Statistical Analysis

All statistical analyses were performed using SAS software v. 9.3 (SAS Institute, Cary, USA). Data were subjected to analysis of variance (ANOVA) and mean comparisons were determined using the Tukey test ($p \leq 0.05$).

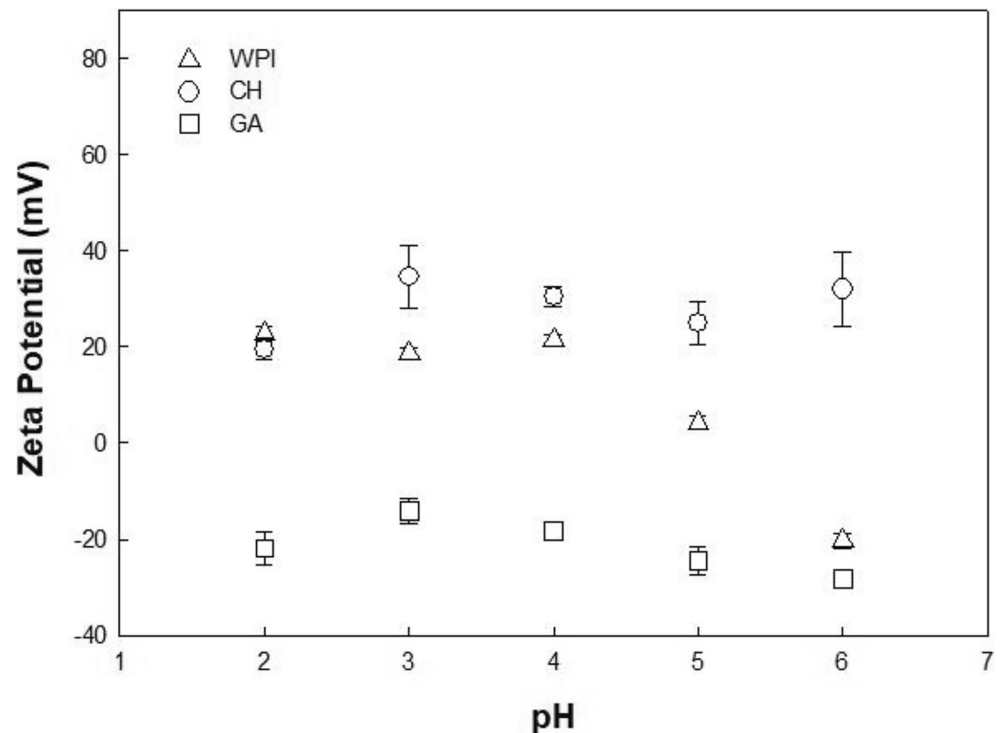
Results and Discussion

Zeta Potential Profile

Zeta potential is related to the surface charge and electric potential in the interfacial double layer of colloidal systems (Retamal Marín et al. 2017; Lu and Gao 2010). The zeta

potential values of CH, GA, and WPI dispersions as a function of pH (2–6) are shown in Fig. 1. The CH and GA dispersions showed positive and negative ζ -potential values, respectively, in all the pH ranges studied. Chitosan is a cationic polysaccharide, which positive ζ -potential values are due to its pKa value (around 6.6), since, for pH values less than 6.6, the amino groups are positively charged (Tan et al. 2016; Espinal-Ruiz et al. 2014). On the other hand, GA is an anionic polysaccharide, since for the pH range studied, the carboxylate groups were negatively charged resulting in negative ζ -potential values (Eratte et al. 2014; Tan et al. 2016). For WPI dispersions, the zeta potential values were positively charged in $\text{pH} \leq 5$ and negative at pH 6. α -Lactalbumin and β -lactoglobulin are important whey proteins with isoelectric points of pH 4.80 and 5.34 (Lee and Hong 2009). The amphoteric nature of the main proteins from WPI is due to the presence of both amino (NH_2) and carboxyl ($-\text{COOH}$) functional groups. Hence, when the pH is lower than the pI, the zeta potential is positive. On the other hand, when the pH is higher than the pI, the negatively charged moieties of $-\text{COO}^-$ outnumber the positively charged moieties of NH_3^+ , resulting in WPI with negative net charge (Chang et al. 2016). Therefore, the WPI/GA and GA/CH complex coacervates were prepared at pH 3.75 and 3.60, according to the results for optimum pH for complex coacervation reported by Eratte et al. (2014) and Butstraen and Salaün (2014), respectively. For GA/CH coacervates, the pH value of 3.6 was higher than the pKa of GA and lower than the pKa of CH, resulting in electrostatic interactions between negative carboxyl groups (–

Fig. 1 Zeta potential (ζ) values for gum Arabic (GA, \square), chitosan (CH, \circ), and whey protein isolate (WPI, Δ) as a function of pH values (2–6)



COO⁻) of GA and positive amino groups (NH₃⁺) for CH. For WPI/GA coacervates, the pH value of 3.75 was higher than the pI of WPI and less than the pKa of GA, resulting in electrostatic interactions between their functional groups. In both cases, the complex coacervation was promoted by electrostatic interactions between opposite biopolymer charges, leading to charge neutralization and consequently the formation of an insoluble complex (Rocha et al. 2014).

Coacervate Yield

The biopolymer mixing ratio influences the biopolymer charge balance, which has a significant effect on the formation of the complex coacervate (Eghbal and Choudhary 2018). Coacervate yield of the equilibrium phase resulted by the mixture of WPI/GA and GA/CH in function of the mass ratio is shown in Fig. 2. For the WPI/GA mass ratio, the coacervate yield increased significantly ($p < 0.05$) until it attained the highest value of 3:1 (w/w), as the result of the maximum electrostatic interaction between positive amino groups (NH₃⁺) of WPI and negative carboxyl groups of GA. From there on, the coacervate yield decreased, confirming maximum electrostatic interactions with coacervate yield reaching 43%. This result is in accordance with Eratte et al. (2014) that reported 3:1 (w/w) as optimum mass ratio between WPI and GA. Weinbreck et al. (2004) studied WPI/GA ratios of 1:1, 2:1, and 8:1 (w/w) and Jain et al. (2015) considered ratios of

1:1, 1:2, and 2:1, and in both studies, it was reported an optimum mass ratio of 2:1. However, none of the investigations studied the mass ratio of 3:1 which was revealed to be the optimum coacervate yield in our research. Estrada-Fernández et al. (2018) also reported the maximum interaction between whey protein concentrate and gum Arabic at a mass ratio of 3:1 (w/w).

In GA/CH complex coacervate system, the highest values of coacervate yield were found at mass ratios of 5:1 and 6:1 (w/w), but without significant differences between them ($p > 0.05$), with the coacervate yields reaching 73%. Other studies have also reported GA/CH mass ratio of 5:1 (w/w) as an optimum ratio to obtain high coacervate yield (Espinosa-Andrews et al. 2007; Butstraen and Salaün 2014; Moschakis et al. 2010; Espinosa-Andrews et al. 2010).

GA/CH coacervate revealed higher yields than WPI/GA coacervates, revealing that interactions polysaccharide-to-polysaccharide were higher than protein-to-polysaccharide. Hence, the WPI/GA and GA/CH with mass ratios of 3:1 and 5:1, respectively, were selected as the optimum ratio to produce complex coacervates in order to act as wall material in the encapsulation of GO.

Rheological Properties of Insoluble Complex

The rheological behavior of the coacervates with and without GO was investigated by shear controlled-stress rheometer

Fig. 2 Coacervate yield profiles of gum Arabic/chitosan (GA/CH) and whey protein isolate/gum Arabic (WPI/GA) complex coacervates for mass ratio (w/w) of 1:1, 2:1, 3:1, 4:1, 5:1, 6:1, and 7:1 at pH 3.66 and 3.75, respectively. The lowercase letters compares mean values of coacervate yield for WPI/GA and uppercase letters compares mean values of coacervate yield for GA/CH. The columns with the same lowercase or uppercase letters are not significantly different ($p < 0.05$) based in Tukey's multiple comparison test

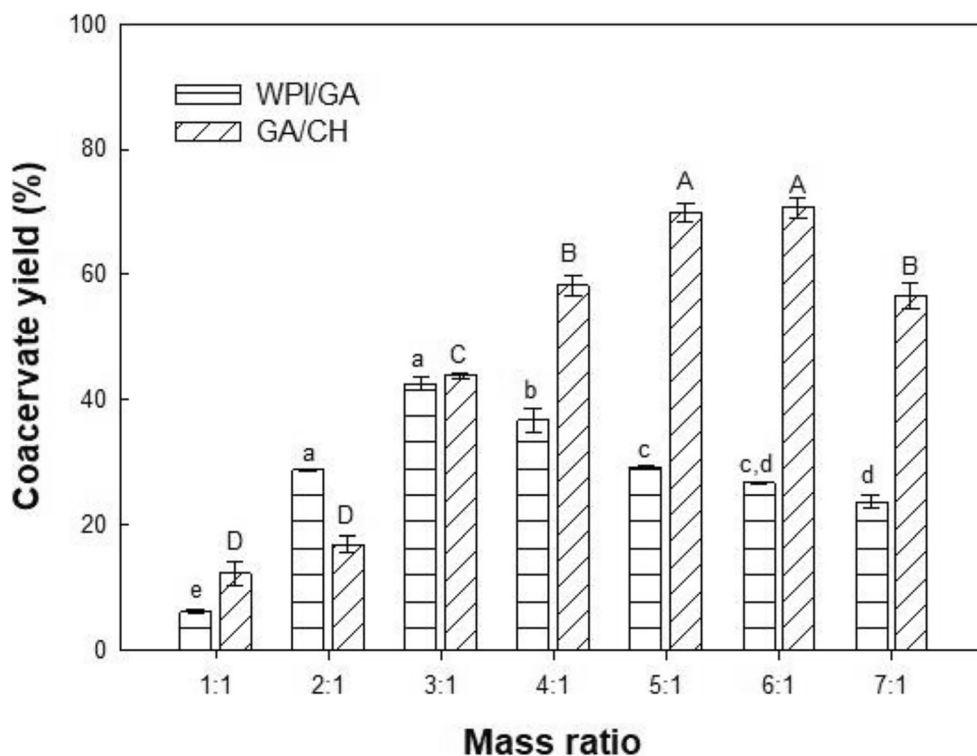


(Fig. 3). The GA/GO/CH and GA/CH coacervates exhibited a typical shear thinning property until shear rate of 15 s^{-1} , exhibiting high viscosity and a pseudoplastic non-Newtonian fluid behavior (Fig. 3). The occurrence of shear thinning is mainly due to the strength of the underlying electrostatic forces that lead to a structural change in the coacervates (Liu et al. 2017). According to Wee et al. (2014), the coacervate shear thinning behavior results as a consequence of the rearrangement and breaking up of its structure formed by attractive electrostatic interactions. However, above shear rate of 15 s^{-1} , the fluid has a behavior similar to the Newtonian fluids, where the viscosity remains constant regardless of shear applied. According to You et al. (2018) for higher shear rates, the new structure formed in complex coacervates is not stable, leading to the disruption of physical bonds and consequent structure breakdown. The WPI/GO/GA also exhibited a typical shear thinning property, but with lower viscosity than GA/GO/CH. Likely, WPI/GA showed shear thinning property with lower viscosity than WPI/GO/GA. Weinbreck et al. (2004) reported a similar result of viscosity behavior for WPI/GA coacervate, where a limited shear thinning property was verified at a low shear rate, indicating a structural change due to the breakup of coacervate physical bonds. In both cases, the viscosity of the coacervates with and without GO has similar behavior and at a higher shear rate, it occurred the disruption of the coacervate structure, resulting in flow curves with similar shapes.

The frequency sweep curves of the coacervates with and without GO are shown in Fig. 4. In all samples, the

magnitudes of loss modulus G'' and storage modulus G' increased when increasing frequency. The GA/CH and GA/GO/CH coacervates showed similar behavior, with greater loss modulus G'' than storage modulus G' for frequency interval until crossover point at 10 Hz, indicating that until this frequency, the coacervates exhibited a viscous behavior (Fig. 4). Above 10 Hz, G' becomes higher than G'' , showing an elastic behavior with gel-like network structures. For GA/CH coacervates, similar results were found by Espinosa-Andrews et al. (2013), where G'' dominating at low frequencies, while G' dominating at higher frequencies.

The GA/CH and GA/GO/CH coacervates revealed similar viscoelasticity properties, indicating that the incorporation of GO did not alter the characteristics of these coacervates. However, the effect of GO addition in coacervate properties was more evident in the systems containing WPI and GA, since not all the GO added was efficiently retained in the structure of the coacervate, as verified in the results of entrapment efficiency (Table 3). For WPI/GA and WPI/GO/GA, in the entire range of frequency, the values of G'' and G' for the WPI/GA and WPI/GO/GA were lower than GA/CH and GA/GO/CH, and the crossover point occurred at higher frequency (80 Hz). This result revealed its more viscous character with weak gel-like network structures. Weinbreck et al. (2004) reported a similar result of frequency sweep test for WPI/GA coacervate elaborated at pH range between 3 and 4.5, where the values of G'' were 3 to 7 times higher than the values of G' . Our results demonstrated that the GO addition mainly weakens

Fig. 3 Viscosity as a function of shear rate between 0 to 100 s^{-1} for complex coacervates with ginger essential oil (GO): Arabic/ginger essential oil/chitosan (GA/GO/CH) and whey protein isolate/ginger essential oil/gum (WPI/GO/GA) and without ginger essential oil (GO): gum Arabic/chitosan (GA/CH) and whey protein isolate/gum Arabic (WPI/GA)

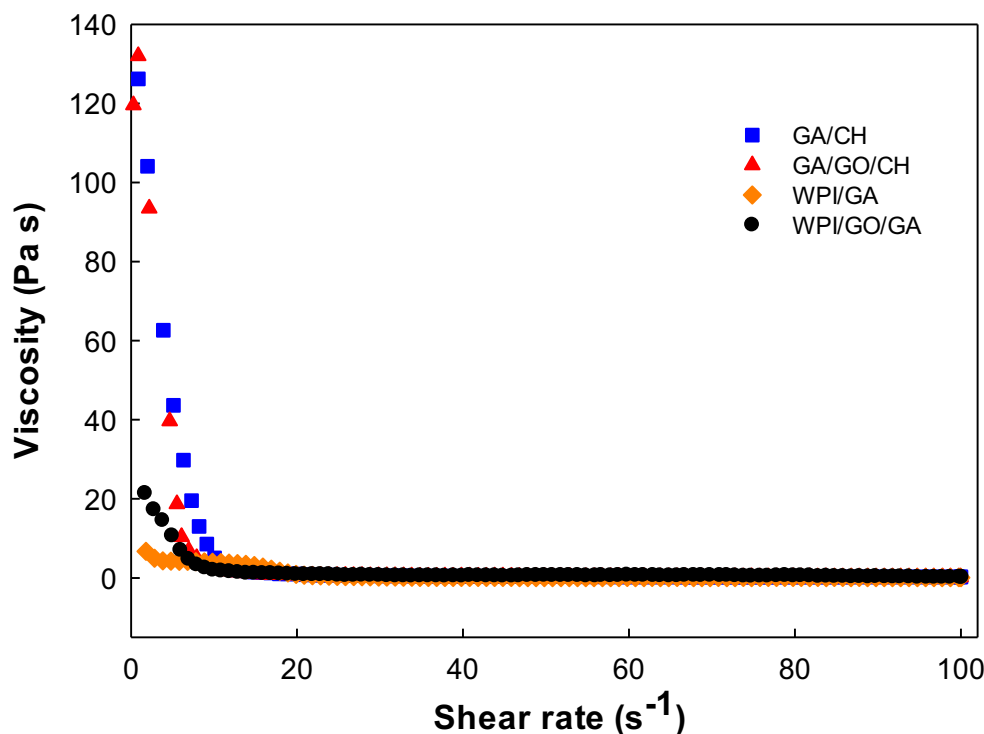
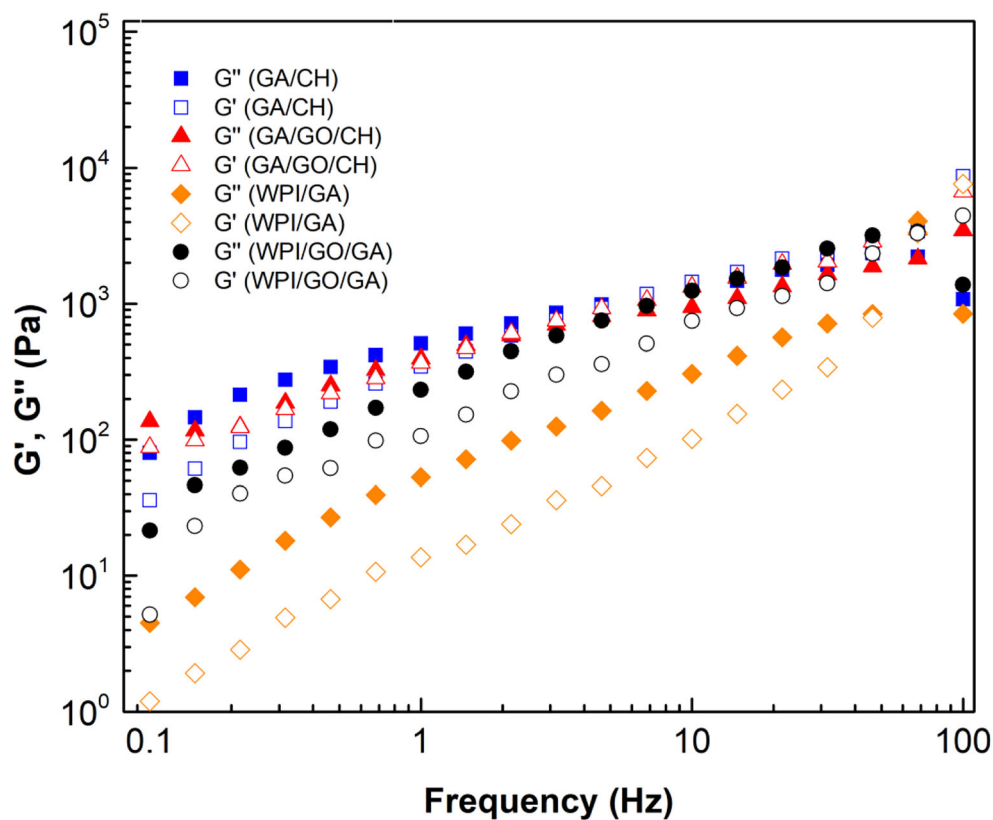


Fig. 4 The viscoelastic modulus (storage moduli (G') and loss moduli (G'') versus frequency for complex coacervates with ginger essential oil (GO): Arabic/ginger essential oil/chitosan (GA/GO/CH) and whey protein isolate/ginger essential oil/gum Arabic (WPI/GO/GA) and without ginger essential oil (GO): gum Arabic/chitosan (GA/CH) and whey protein isolate/gum Arabic (WPI/GA)



the electrostatic forces between biopolymers chains, causing a decrease in both moduli.

These results demonstrated that GA/CH and GA/GO/CH coacervates are more concentrated than WPI/GA and WPI/GO/GA. According to Steffe (1996), concentrated solutions display crossover lines between G' and G'' at the middle of the frequency range and showed a clear evidence of solid-like behavior at higher frequencies.

Creep and Recovery

Figure 5 shows the compliance results (Eq. 2) for the creep and recovery behaviors of complex coacervates with and without GO. The creep test represents a time interval from 0 to 90 s and the recovery test represents a time interval from 90 to 180 s. According to Huang et al. (2016), in the creep-recovery test, samples with stronger structure have lower J_t values, while samples with weaker structure have higher J_t values.

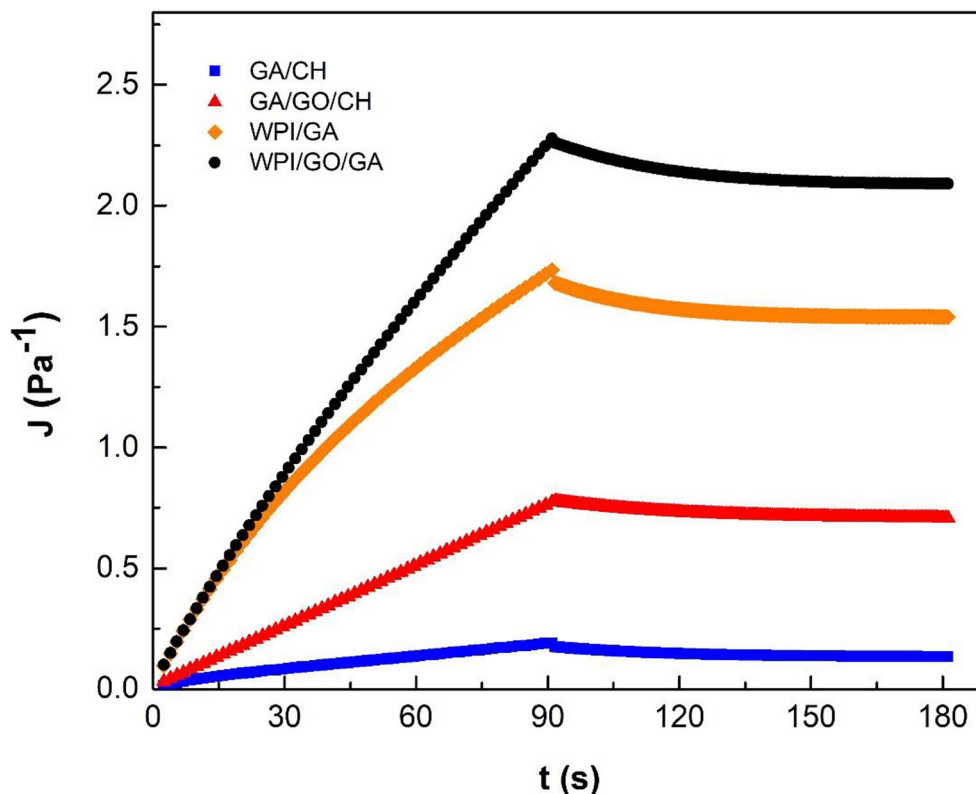
The GA/CH coacervate revealed a curve with less compliant behavior, indicating the formation of a stronger network structure. The GO addition increased the compliance behavior of GA/CH, revealing that the presence of GO in the complex coacervate mainly interfered in the electrostatic interactions between positively charged amino groups ($-\text{NH}_3^+$) present in CH chains available to interact with negatively charged carboxyl groups ($-\text{COO}^-$) in the GA. Similar behavior was verified in

system with WPI and GA. The results of compliance behavior suggested that the GO incorporation alters the characteristics and structure of coacervates. The Burgers model was used in order to predict the behavior of the creep phase and provide an approximate description of the linear viscoelastic behavior through the static test. The four parameters G_0 , G_1 , η_0 , and η_1 obtained by Burgers model are listed in Table 1. In all the cases, the coefficients of determination (R^2) were higher than 0.99, indicating that the Burgers model was adequate to describe coacervate creep behavior, which reflects the characteristic of their internal structure (Karaman et al. 2012). The instantaneous shear modulus G_0 provides results of intensity degree of elastic strength on the bonds present in the interfacial network structure (Huang et al. 2016).

In the creep phase, the constant stress applied caused a transient response that includes elastic and viscous properties, contributing to the general viscoelastic behavior (Huang et al. 2016). The creep phase mainly contains three periods: instantaneous response, retarded elastic behavior, and long-time viscous flow (Dogan et al. 2013). The coacervates showed a curve shape with typical periods of long-time viscous flow larger than the retarded elastic behavior (Dogan et al. 2013).

The GA/CH and GA/GO/CH presented higher value for G_0 ($p < 0.05$) due to the formation of a strength network structure than coacervates with WPI and GA. This behavior is in accordance with the results verified in dynamic test with superior storage and the loss modulus values (Fig. 4). In both cases, the

Fig. 5 Compliance versus time in creep and recovery test of (■, blue) gum Arabic/chitosan (GA/CH), (▲, red) gum Arabic/ginger essential oil/chitosan (GA/GO/CH), (◆, orange) whey protein isolate/gum Arabic (WPI/GA), and (●, black) whey protein isolate/ginger essential oil/gum Arabic (WPI/GO/GA) complex coacervates



G_0 values of coacervates decreased with GO addition, which means a decrease in elastic strength of the coacervate network structure. In both cases, the GO addition caused an increase in the value of the retarded elastic modulus G_1 . The GO addition caused a decrease in the internal viscosity η_1 associated with Kelvin–Voigt dashpot for GA/CH coacervate and increased for WPI/GA. The viscoelastic properties of the coacervates are influenced by the bond strength, which results in their network structure (Tavares and Noreña 2018). The residual viscosity of the Maxwell dashpot η_0 values decreased with GO addition, indicating a lower resistance to the flow. To our knowledge, no reports exist yet on the study of creep behavior of WPI/GA

and GA/CH complex coacervates, and for this reason, it was not possible to make a comparison of our results.

The recovery phenomenon was monitored in the end of the creep period, where the constant stress applied was zero. In this phase, only purely elastic systems have the capacity for complete regeneration (Yilmaz et al. 2012). Parameters estimated of J_∞ , J_{1R} , C , J_{max} , and final percentage recovery of samples (%R) are shown in Table 2. For all coacervates analyzed, coefficients of determination (R^2) were higher than 0.98, confirming the excellent fitting quality of the exponential decay function (Eq. 4) in describing the recovery phase.

Table 1 Instantaneous shear modulus of the Maxwell unit (G_0), shear modulus of Kelvin–Voigt (G_1), residual viscosity (dashpot contribution) of the Maxwell element (η_0), and internal viscosity (dashpot contribution) of Kelvin–Voigt unit (η_1) parameters obtained from the data fit according

to the Burgers model of creep behavior (Eq. 3) for gum Arabic/ginger essential oil/chitosan (GA/GO/CH), whey protein isolate/ginger essential oil/gum Arabic (WPI/GO/GA), gum Arabic/chitosan (GA/CH), and whey protein isolate/gum Arabic (WPI/GA) complex coacervates

Complex	Burgers model parameters				
	G_0 (Pa)	G_1 (Pa)	η_0 (Pa s)	η_1 (Pa s)	R^2
GA/CH	226.51 ± 19.91 ^a	36.67 ± 1.09 ^b	15.53 ± 0.47 ^c	310.01 ± 23.75 ^a	0.9998
GA/GO/CH	197.32 ± 18.15 ^a	183.60 ± 18.10 ^a	0.65 ± 0.02 ^d	51.87 ± 5.14 ^b	0.9985
WPI/GA	75.75 ± 9.89 ^b	1.20 ± 0.03 ^d	80.95 ± 10.19 ^a	40.21 ± 0.71 ^d	0.9999
WPI/GO/GA	48.12 ± 4.37 ^c	1.87 ± 0.39 ^c	27.38 ± 5.41 ^b	73.82 ± 3.03 ^c	0.9999

Different letters in the same column indicate values that are significantly different ($p < 0.05$) based on Tukey’s multiple comparison test

Table 2 Maximum compliance, J_{\max} , compliance of the Maxwell dashpot, J_{∞} , Kelvin–Voigt element, J_{1R} , and parameters B and C of the systems obtained from fitting of the empirical model (Eq. 4) for gum Arabic/ginger essential oil/chitosan (GA/GO/CH), whey protein isolate/

ginger essential oil/gum Arabic (WPI/GO/GA), gum Arabic/chitosan (GA/CH), and whey protein isolate/gum Arabic (WPI/GA) complex coacervates. The correlation coefficients (R^2) and final percentage recovery (% R) are also represented

Complex	J_{∞} (Pa ⁻¹)	J_{\max} (Pa ⁻¹)	J_{1R} (Pa ⁻¹)	B	C	% R	R^2
GA/CH	0.1336 ± 0.0014 ^d	0.1885 ± 0.0029 ^d	0.8298 ± 0.0717 ^c	0.0147 ± 0.0010 ^b	1.1770 ± 0.1013 ^c	29.11 ± 0.35 ^b	0.9843
GA/GO/CH	0.7057 ± 0.0024 ^c	0.7899 ± 0.0001 ^c	1.2371 ± 0.0870 ^b	0.0172 ± 0.0010 ^a	1.1310 ± 0.0021 ^c	22.31 ± 0.28 ^c	0.9902
WPI/GA	1.5405 ± 0.0025 ^b	1.7230 ± 0.0050 ^b	1.7331 ± 0.0431 ^a	0.0011 ± 0.0001 ^c	1.7050 ± 0.0010 ^b	37.01 ± 0.07 ^a	0.9805
WPI/GO/GA	2.0890 ± 0.0030 ^a	2.2781 ± 0.0061 ^a	1.2580 ± 0.0120 ^b	0.0007 ± 0.0001 ^d	1.7601 ± 0.1501 ^a	8.30 ± 0.11 ^d	0.9834

Different letters in the same column indicate values that are significantly different ($p < 0.05$) based on Tukey's multiple comparison test

The GO addition resulted in complex coacervates with significantly ($p < 0.05$) superior J_{∞} (residual compliance corresponding to the permanent deformation of the Maxwell dashpot) and maximum compliance J_{\max} suggesting a weaker and softer network structure. These results are consistent with the ones obtained in the creep phase and help to clarify the results of the oscillatory frequency sweep test where the behavior was practically similar at a higher frequency. The values of parameter C (recovery speed of the system related to the curvature shape) did not differ significantly ($p > 0.05$) for GA/CH and GA/GO/CH. However, the GO incorporation in the WPI/GA resulted in coacervates with significantly ($p < 0.05$) higher C value. The WPI/GA and WPI/GO/GA coacervates revealed inferior values for B (recovery speed of the system) than GA/CH and GA/GO/CH, mainly due to their lower magnitude phase (Tavares and Noreña 2018). According to Dogan et al. (2013), samples with recovery percentage equal to zero indicate liquid behavior. The percentage recovery (% R) of the coacervates decreased with GO addition, indicating a viscous behavior for this coacervates. The coacervates without GO presented higher % R values due to its superior capacity for structural recovery, suggesting stronger interaction between the biopolymers (Tavares and Noreña 2018).

Moisture Content, Hygroscopicity, Solubility, and Entrapment Efficiency

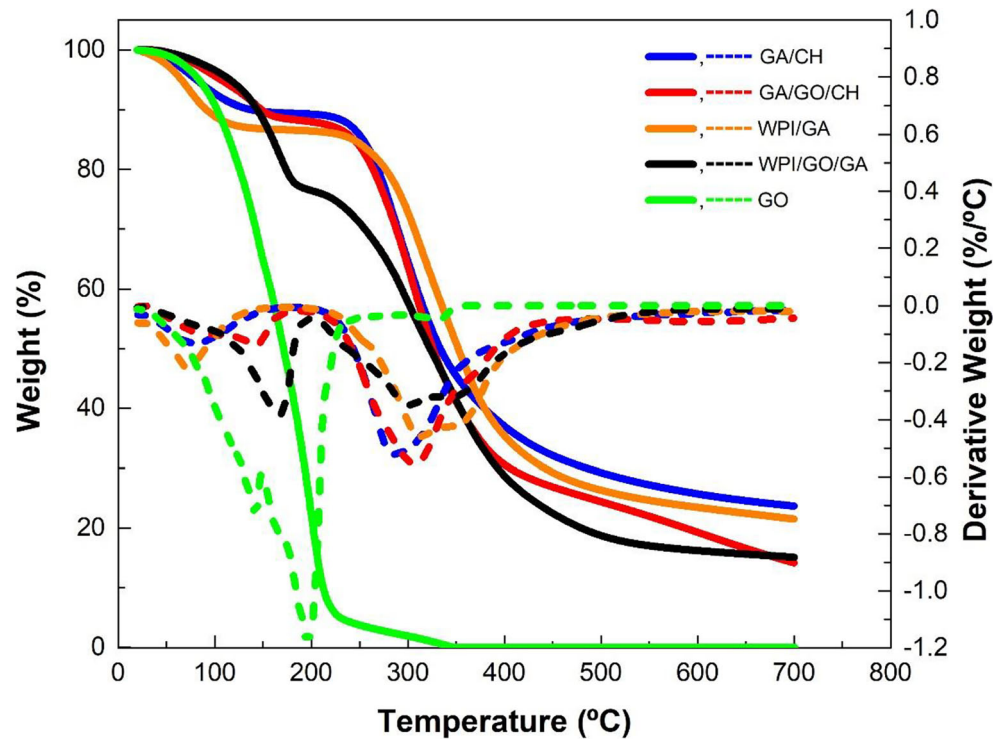
The coacervates with and without incorporation of GO were subject to freeze drying to obtain microparticle powders, aiming its better preservation, ease of handling, transport, and storage. The moisture content is an important property of the powders, which relates to the storage stability and shelf life. The moisture content of the powders ranged from 3.04 to 8.02%. The lowest moisture content values were obtained in the microparticles with ginger essential oil contents. These results are in accordance with the TGA curves reported in Fig. 6. The hygroscopicity of the powders ranged from 8.75 to 9.65% (Table 3). Powders with hygroscopic values higher than 15.1% are considered of high hygroscopicity (Zotarelli

et al. 2017). The coacervates with GO showed lower hygroscopicity than coacervates without GO, mainly due to the hydrophobic nature of GO compounds (Fernandes et al. 2014). The WPI/GO/GA microparticle revealed lower hygroscopic value than GA/GO/CH, mainly due to some unprotected GO in the powder superficies, reducing the water adsorptions from the relatively moist environment (Table 3).

In the food industry, powders are required to present good solubility in water in order to increase their range of application. In our study, all samples showed low solubility in water (Table 3). This result is characteristic of powders obtained by the complex coacervation method that allows the formation of water insoluble complex (Rocha-Selmi et al. 2013). However, the powders obtained by complex coacervation allow gradual and controlled release when in contact with aqueous medium and also enable changes in the ionic strength of the medium (Comunian et al. 2013). Other studies demonstrated that the encapsulation of ginger essential oil by spray-drying process resulted in powders with higher solubility, revealing an alternative in the application where high solubility in water is required (Fernandes et al. 2016b). The solubility value of powders obtained by GA/CH complex coacervate decreased significantly ($p < 0.05$) with the incorporation of GO. Nevertheless, this effect was not significantly ($p > 0.05$) for powders of WPI/GA.

The results of entrapment efficiency (EE) of GO encapsulation are shown in Table 3. The GA/GO/CH microparticles showed higher EE mainly due to its better physical-chemical properties and high coacervate yield, as verified in the above sections. Fernandes et al. (2016a) reported GO encapsulation efficiency ranging from 17 to 30% using cashew gum and inulin as wall materials. In another study, Fernandes et al. (2016b) reported encapsulation efficiency ranging from 48 to 93% using Arabic, maltodextrin, and inulin as wall materials. In both studies, the microparticles were obtained by spray-drying process. Therefore, our results of entrapment efficiency revealed that the mechanism of complex coacervation followed by freeze drying is a good alternative to the encapsulation of sensitive compounds such as volatile components of GO.

Fig. 6 Thermogravimetric analysis (TGA, solid line) and differential thermogravimetric analysis (DTGA, dashed line) curves of the bulk ginger essential oil (GO) and microparticle powders obtained by the freeze-drying process: gum Arabic/chitosan (GA/CH), gum Arabic/ginger essential oil/chitosan (GA/GO/CH), whey protein isolate/gum Arabic (WPI/GA), and whey protein isolate/ginger essential oil/gum Arabic (WPI/GO/GA)



Thermogravimetric Analysis

Thermogravimetric analysis (TGA) and their corresponding derivative weight loss (DTGA) curves for pure GO and dried coacervates with and without GO are shown in Fig. 6. The TGA curve of pure GO shows a rapid and marked reduction in the mass from 100 to 200 °C, associated to the evaporation and decomposition of GO compounds (da Silva et al. 2018). Similar result of thermal stability of GO was also reported by Fernandes et al. (2016b). The thermal decomposition process of all dried coacervates occurred in three steps: the first, with weight loss from 40 to 105 °C, is associated with the loss of unprotected volatile oil and the bound water, representing weight loss of 7.78, 4.86, 10.01, and 3.01% for GA/CH, GA/GO/CH, WPI/GA, and WPI/GO/GA, respectively. The second, with weight loss from 105 to 400 °C, is attributed to

decompositions/depolymerization of functional wall materials and volatilization of the GO that became unprotected, representing weight loss of 55.07, 64.41, 52.93, and 66.26% for GA/CH, GA/GO/CH, WPI/GA, and WPI/GO/GA, respectively. The decomposition of WPI begins with the cleavage of S–S, O–N, and O–O linkages and with the breakdown of covalent peptide bonds in the amino acid residues (Azizi et al. 2018). The CH degradations are attributed to the depolymerization and degradation of CH D-glucosamine and N-acetyl-D-glucosamine units, respectively (Gámiz-González et al. 2017). The GA degradation is due to the carbohydrate ring dehydration, decomposition, and depolymerization (Fernandes et al. 2016b). The third, up to 500 °C until 700 °C, is attributed to the decomposition of residual carbon groups present in the structure of these biopolymers, representing weight loss of 5.69, 10.23, 4.74, and 4.02% for

Table 3 Physical-chemical properties of dried coacervates with ginger essential oil (GO): Arabic/ginger essential oil/chitosan (GA/GO/CH) and whey protein isolate/ginger essential oil/gum Arabic (WPI/GO/GA) and

without ginger essential oil (GO): gum Arabic/chitosan (GA/CH) and whey protein isolate/gum Arabic (WPI/GA)**

Powders	Hygroscopicity (%)	Moisture content (%)	Solubility (%)	Entrapment efficiency (%)
GA/CH	9.65 ± 0.05 ^a	6.01 ± 0.32 ^b	39.37 ± 0.50 ^a	--
GA/GO/CH	8.75 ± 0.33 ^b	3.04 ± 0.13 ^c	33.90 ± 0.01 ^b	81.98 ± 1.77 ^a
WPI/GA	8.95 ± 0.47 ^b	8.02 ± 0.28 ^a	13.70 ± 0.19 ^c	--
WPI/GO/GA	6.64 ± 0.04 ^c	3.10 ± 0.21 ^c	13.39 ± 0.24 ^c	55.31 ± 3.02 ^b

**Values (mean ± SD) in a column with different letters are significantly different (*p* < 0.05) based on Tukey’s multiple comparison test

GA/CH, GA/GO/CH, WPI/GA, and WPI/GO/GA, respectively. The TGA curves of microparticles confirmed that the encapsulation allows to protect the heat-sensitive compounds present in GO. The TGA curves of GA/CH and GA/GO/CH showed similar shape, which proved an efficient encapsulation of the GO. However, the shapes of TGA curves of WPI/GA and WPI/GO/GA were different. The TGA curves of WPI/GO/GA microparticles showed mass loss of 10% from 150 and 200 °C, mainly due to the evaporation and degradation of non-encapsulated GO present in the surface of the powders. This result accords to the one obtained in the determination of the entrapment efficiency of GO, which revealed superior GA/CH capacity to GO encapsulation (Table 3). Therefore, the TGA curves of dried coacervates with GO showed clearly that the wall materials contributed to a significant increase in the thermal stability of GO.

Morphology

Scanning electron microscopy (SEM) was used to evaluate and compare the morphological structures of dried coacervates with and without GO (Fig. 7). All the SEM images showed powders

with larger size and irregular shapes resembling broken glass or a flake-like structure. The images showed no evidence of cracking or fissures in the microparticles superficies. However, both WPI/GO/GA and GA/GO/CH microparticles revealed the presence of significant microcavities and pores on their superficies as a result of smaller ice crystal formation in the emulsion freezing step, which sublimed during freeze-drying process, leading to the formation of a porous structure (Anandharamakrishnan et al. 2010).

FTIR Analysis

The infrared spectra of the wall materials (GA, CH, and WPI) and dried coacervates without GO (GA/CH and WPI/GA) are shown in Fig. 8(a). The FTIR spectrum of GA showed a typical band at 3320 cm^{-1} for O–H stretching, 2922 cm^{-1} for C–H stretching, 1641 cm^{-1} for C=O stretching, 1400 cm^{-1} for C–H bending, and 1073 cm^{-1} for C–O stretching. CH showed a broad band at 3330 cm^{-1} for O–H stretching vibrations, which overlapped the stretching band of N–H (Tan et al. 2016). It was also verified CH bands with characteristic at 2993 cm^{-1} for C–H stretching, 1167 cm^{-1} for C–O–C

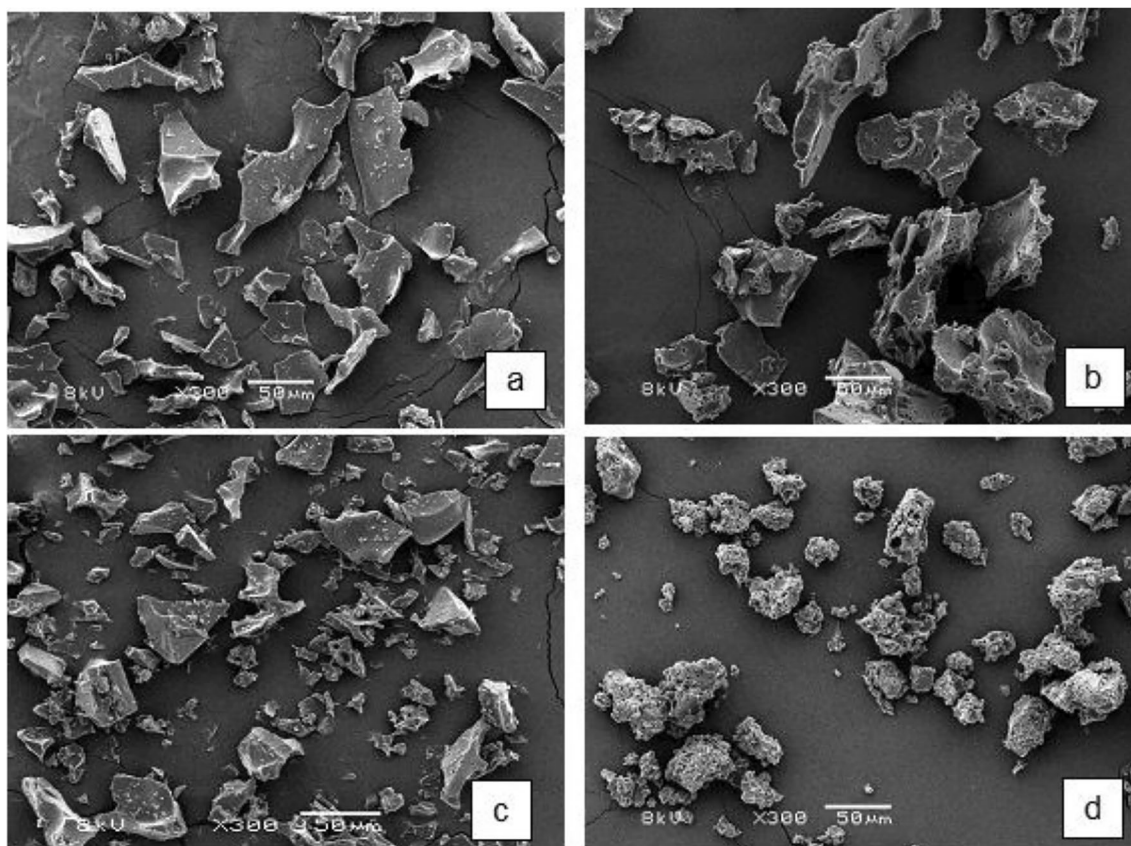
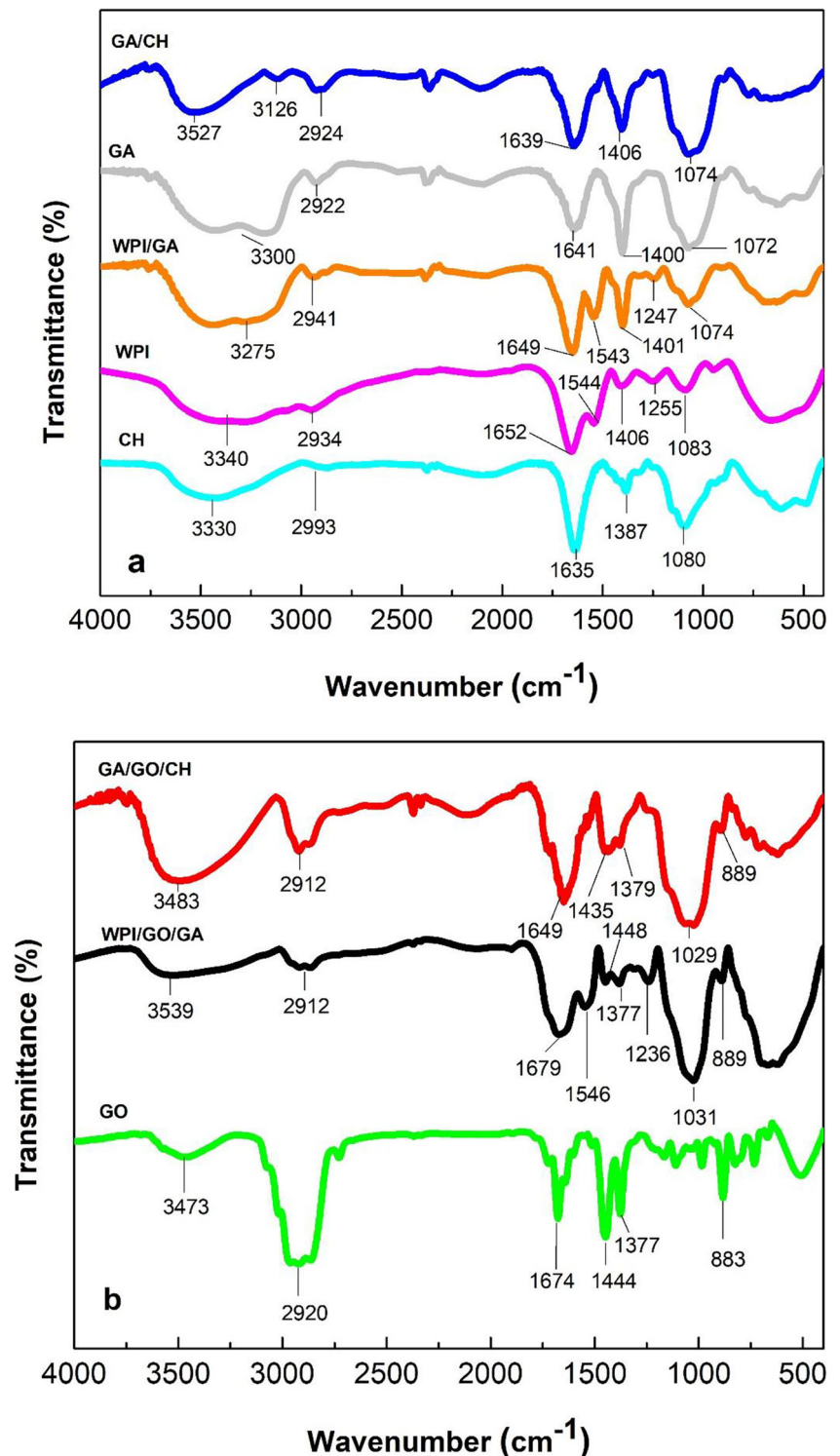


Fig. 7 SEM micrographs of (a) gum Arabic/chitosan (GA/CH), (b) gum Arabic/ginger essential oil/chitosan (GA/GO/CH), (c) whey protein isolate/gum Arabic (WPI/GA), and (d) whey protein isolate/ginger essential oil/gum Arabic (WPI/GO/GA) microparticles at magnification of $\times 300$

Fig. 8 FTIR spectrum of (a) raw wall materials: gum Arabic (GA), chitosan (CH), whey protein isolate (WPI); dried coacervates without ginger essential oil (GO): gum Arabic/chitosan (GA/CH) and whey protein isolate/gum Arabic (WPI/GA); (b) bulk ginger essential oil (GO) and microparticles within ginger essential oil (GO): gum Arabic/ginger essential oil/chitosan (GA/GO/CH), and whey protein isolate/ginger essential oil/gum Arabic (WPI/GO/GA)



symmetrical stretching, 1080 cm^{-1} for C–O stretching, 1410 cm^{-1} for O–H and C–H vibrations, and 1635 cm^{-1} corresponding to amide I (C–O and C–N stretching) (Huang et al. 2012). WPI showed a typical band at 3340 cm^{-1} for O–H and N–H stretching vibrations, 2934 cm^{-1} for C–H stretching, 1652 cm^{-1} for C=O stretching vibrations and amide I,

1544 cm^{-1} corresponding to amide II, 1406 cm^{-1} for N–H bending and C–N stretching vibrations, 1083 cm^{-1} for C–O–C stretching vibrations, and 1255 cm^{-1} resulting band, mainly due to the borderline between the random coil and β -sheet secondary structure present in WPI (Tavares and Noreña 2018; Cai and Singh 1999). During complex coacervation,

carboxyl groups in GA interact with amino groups in WPI and CH to form a complex that contains amide groups. The GA/CH and WPI/GA showed a broad band between 3000 and 3700 attributed to NH₂ and OH group stretching vibration (Espinosa-Andrews et al. 2010). This result demonstrated that the enhancement of hydrogen bonding is also involved in the interactions between the biopolymers and the consequent formation of complex coacervates. Huang et al. (2012) reported similar results in the complex coacervation resulted by electrostatic interactions between soybean and chitosan. The GA/CH and WPI/GA spectra also showed band characteristics of individual biopolymers, confirming the presence of both biopolymers in the dried coacervate. These results were also reported by Tan et al. (2016), which means that both physical and chemical interaction occurred between the functional groups of biopolymers.

The FTIR spectrum of pure GO showed a typical band at 3200 cm⁻¹ for O–H stretching, 2922 cm⁻¹ for C–H stretching, 1674 cm⁻¹ for C=C stretches, 1446 cm⁻¹ for C=C–C=C stretches, 1377 cm⁻¹ associated with CH₃ group bending, and 883 cm⁻¹ for C–H bond stretching (Fig. 8(b)). Da Silva et al. (2018) and Fernandes et al. (2016b) reported a similar GO FTIR spectrum and attributed this band characteristic to the structure of α -zingiberene (major compound of the essential oil). Despite the presence of reduced amount of GO in the dried coacervates, all the above characteristic peaks appear at the same wavenumber in the spectra of WPI/GO/GA and GA/GO/CH microparticles. These results indicate no modification or interaction between active groups of GO and functional groups of wall materials. Thereby, the FTIR spectra confirms that no new chemical bonds were formed, indicating that compounds of GO might be encapsulated into coacervates by physical interactions.

Conclusions

This study demonstrated that the use of wall materials resulted by a complex mixture between gum Arabic (GA)/whey protein isolate (WPI) and gum Arabic (GA)/chitosan (CH) allowed to keep the proprieties and stability of ginger essential oil. The pH and biopolymer's mass ratio was an important factor in the complex coacervation process; thus, the optimum complex coacervation between WPI/GA and GA/CH occurred at the mass ratio of 3:1 (w/w) and 5:1 (w/w), respectively. The dynamic rheological measurement indicated that the coacervates have a viscous behavior ($G'' > G'$) at lower frequency and elastic behavior ($G' > G''$) at higher frequency. The creep-recovery test showed that the incorporation of GO in the complex coacervate resulted in coacervates with weaker and softer network structure. The physical-chemical properties of the dried coacervates and wall materials used had influence in the GO encapsulation. FTIR analyses confirmed the

encapsulation of ginger essential oil. TGA analyses confirmed that the encapsulation allows to protect the heat-sensitive compounds present in ginger essential oil. The SEM analysis showed microparticles with flake-like structure and there were no evidence of cracking or fissures in the surface. The GA/CH complex used as wall materials had the best potential to be successfully applied in the encapsulation of ginger essential oil. Further studies should be carried out in order to study the oxidative stability of GO in microparticles and to determine the potential applications of microparticles as ingredients in the elaboration of several food products such as chewing gum, soup, and bakery products.

Funding Information The authors thank the financial support from CNPq and FAPERGS. Especially thanks to Primex (Siglufjörður, Iceland) and Arla Foods Ingredients for donating chitosan and whey proteins isolates, respectively. Loleny Tavares also thanks CAPES/CNPq-Programa Estudantes-Convênio de Pós-Graduação (PEC-PG) for scholarship funding.

Compliance with Ethical Standards

Conflict of Interest The authors declare that they have no conflict of interest.

References

- Anandharamakrishnan, C., Rielly, C. D., & Stapley, A. G. (2010). Spray-freeze-drying of whey proteins at sub-atmospheric pressures. *Dairy Science & Technology*, *90*(2–3), 321–334.
- AOAC. (1990). *Official methods of analysis*. Washington, DC: Association of Official Analytical Chemists.
- Augusto, P. E. D., Ibarz, A., & Cristianini, M. (2013). Effect of high pressure homogenization (HPH) on the rheological properties of tomato juice: creep and recovery behaviours. *Food Research International*, *54*(1), 169–176.
- Azizi, M., Kierulf, A., Lee, M. C., & Abbaspourrad, A. (2018). Improvement of physicochemical properties of encapsulated echium oil using nanostructured lipid carriers. *Food Chemistry*, *246*, 448–456.
- Bellik, Y. (2014). Total antioxidant activity and antimicrobial potency of the essential oil and oleoresin of *Zingiber officinale* Roscoe. *Asian Pacific Journal of Tropical Disease*, *4*(1), 40–44.
- Butstraen, C., & Salaün, F. (2014). Preparation of microcapsules by complex coacervation of gum Arabic and chitosan. *Carbohydrate Polymers*, *99*, 608–616.
- Cai, Y., & Corke, H. (2000). Production and properties of spray-dried amaranthus betacyanin pigments. *Journal of Food Science*, *65*(7), 1248–1252.
- Cai, S., & Singh, B. R. (1999). Identification of β -turn and random coil amide III infrared bands for secondary structure estimation of proteins. *Biophysical Chemistry*, *80*(1), 7–20.
- Cano-Chauca, M., Stringheta, P., Ramos, A., & Cal-Vidal, J. (2005). Effect of the carriers on the microstructure of mango powder obtained by spray drying and its functional characterization. *Innovative Food Science & Emerging Technologies*, *6*(4), 420–428.
- Castro-Rosas, J., Ferreira-Grosso, C. R., Gómez-Aldapa, C. A., Rangel-Vargas, E., Rodríguez-Marín, M. L., Guzmán-Ortiz, F. A., & Falfán-Cortés, R. N. (2017). Recent advances in microencapsulation

- of natural sources of antimicrobial compounds used in food—a review. *Food Research International*, 102, 575–587.
- Chang, P. G., Gupta, R., Timilsena, Y. P., & Adhikari, B. (2016). Optimisation of the complex coacervation between canola protein isolate and chitosan. *Journal of Food Engineering*, 191, 58–66.
- Comunian, T. A., Thomazini, M., Alves, A. J. G., de Matos Junior, F. E., de Carvalho Balieiro, J. C., & Favaro-Trindade, C. S. (2013). Microencapsulation of ascorbic acid by complex coacervation: protection and controlled release. *Food Research International*, 52(1), 373–379.
- da Silva, F. T., da Cunha, K. F., Fonseca, L. M., Antunes, M. D., El Halal, S. L. M., Fiorentin, Á. M., et al. (2018). Action of ginger essential oil (*Zingiber officinale*) encapsulated in proteins ultrafine fibers on the antimicrobial control in situ. *International Journal of Biological Macromolecules*, 118(Pt A), 107–115.
- Dogan, M., Kayacier, A., Tokar, Ö. S., Yilmaz, M. T., & Karaman, S. (2013). Steady, dynamic, creep, and recovery analysis of ice cream mixes added with different concentrations of xanthan gum. *Food and Bioprocess Technology*, 6(6), 1420–1433.
- Dolz, M., Hernández, M., & Delegido, J. (2008). Creep and recovery experimental investigation of low oil content food emulsions. *Food Hydrocolloids*, 22(3), 421–427.
- Eghbal, N., & Choudhary, R. (2018). Complex coacervation: encapsulation and controlled release of active agents in food systems. *LWT - Food Science and Technology*, 90, 254–264.
- Eratte, D., Wang, B., Dowling, K., Barrow, C. J., & Adhikari, B. P. (2014). Complex coacervation with whey protein isolate and gum arabic for the microencapsulation of omega-3 rich tuna oil. *Food & Function*, 5(11), 2743–2750.
- Eratte, D., McKnight, S., Gengenbach, T. R., Dowling, K., Barrow, C. J., & Adhikari, B. P. (2015). Co-encapsulation and characterisation of omega-3 fatty acids and probiotic bacteria in whey protein isolate–gum Arabic complex coacervates. *Journal of Functional Foods*, 19, 882–892.
- Eratte, D., Dowling, K., Barrow, C. J., & Adhikari, B. P. (2017). In-vitro digestion of probiotic bacteria and omega-3 oil co-microencapsulated in whey protein isolate–gum Arabic complex coacervates. *Food Chemistry*, 227, 129–136.
- Espinal-Ruiz, M., Parada-Alfonso, F., Restrepo-Sánchez, L.-P., Narváez-Cuenca, C.-E., & McClements, D. J. (2014). Impact of dietary fibers [methyl cellulose, chitosan, and pectin] on digestion of lipids under simulated gastrointestinal conditions. *Food & Function*, 5(12), 3083–3095.
- Espinosa-Andrews, H., Báez-González, J. G., Cruz-Sosa, F., & Vernon-Carter, E. J. (2007). Gum arabic–chitosan complex coacervation. *Biomacromolecules*, 8(4), 1313–1318.
- Espinosa-Andrews, H., Sandoval-Castilla, O., Vázquez-Torres, H., Vernon-Carter, E. J., & Lobato-Calleros, C. (2010). Determination of the gum Arabic–chitosan interactions by Fourier transform infrared spectroscopy and characterization of the microstructure and rheological features of their coacervates. *Carbohydrate Polymers*, 79(3), 541–546.
- Espinosa-Andrews, H., Enríquez-Ramírez, K. E., García-Márquez, E., Ramírez-Santiago, C., Lobato-Calleros, C., & Vernon-Carter, J. (2013). Interrelationship between the zeta potential and viscoelastic properties in coacervates complexes. *Carbohydrate Polymers*, 95(1), 161–166.
- Estrada-Fernández, A. G., Román-Guerrero, A., Jiménez-Alvarado, R., Lobato-Calleros, C., Alvarez-Ramirez, J., & Vernon-Carter, E. J. (2018). Stabilization of oil-in-water-in-oil (O1/W/O2) Pickering double emulsions by soluble and insoluble whey protein concentrate–gum Arabic complexes used as inner and outer interfaces. *Journal of Food Engineering*, 221, 35–44.
- Ezhilarasi, P., Karthik, P., Chhanwal, N., & Anandharamakrishnan, C. (2013). Nanoencapsulation techniques for food bioactive components: a review. *Food and Bioprocess Technology*, 6(3), 628–647.
- Fan, Q., Wang, L., Song, Y., Fang, Z., Subirade, M., & Liang, L. (2017). Partition and stability of resveratrol in whey protein isolate oil-in-water emulsion: impact of protein and calcium concentrations. *International Dairy Journal*, 73, 128–135.
- Fernandes, R. V., Marques, G. R., Borges, S. V., & Botrel, D. A. (2014). Effect of solids content and oil load on the microencapsulation process of rosemary essential oil. *Industrial Crops and Products*, 58, 173–181.
- Fernandes, R. V., Borges, S. V., Silva, E. K., da Silva, Y. F., de Souza, H. J. B., do Carmo, E. L., et al. (2016a). Study of ultrasound-assisted emulsions on microencapsulation of ginger essential oil by spray drying. *Industrial Crops and Products*, 94, 413–423.
- Fernandes, R. V., Botrel, D. A., Silva, E. K., Borges, S. V., de Oliveira, C. R., Yoshida, M. I., et al. (2016b). Cashew gum and inulin: new alternative for ginger essential oil microencapsulation. *Carbohydrate Polymers*, 153, 133–142.
- Fernandes, R. V., Silva, E. K., Borges, S. V., de Oliveira, C. R., Yoshida, M. I., da Silva, Y. F., et al. (2017). Proposing novel encapsulating matrices for spray-dried ginger essential oil from the whey protein isolate–inulin/maltodextrin blends. *Food and Bioprocess Technology*, 10(1), 115–130.
- Gámiz-González, M., Correia, D. M., Lanceros-Mendez, S., Sencadas, V., Ribelles, J. G., & Vidaurte, A. (2017). Kinetic study of thermal degradation of chitosan as a function of deacetylation degree. *Carbohydrate Polymers*, 167, 52–58.
- Huang, G. Q., Sun, Y. T., Xiao, J. X., & Yang, J. (2012). Complex coacervation of soybean protein isolate and chitosan. *Food Chemistry*, 135(2), 534–539.
- Huang, J., Zeng, S., Xiong, S., & Huang, Q. (2016). Steady, dynamic, and creep-recovery rheological properties of myofibrillar protein from grass carp muscle. *Food Hydrocolloids*, 61, 48–56.
- Jain, A., Thakur, D., Ghoshal, G., Katore, O. P., & Shivhare, U. S. (2015). Microencapsulation by complex coacervation using whey protein isolates and gum acacia: an approach to preserve the functionality and controlled release of β -carotene. *Food and Bioprocess Technology*, 8(8), 1635–1644.
- Jakribettu, R. P., Boloor, R., Bhat, H. P., Thaliath, A., Haniadka, R., Rai, M. P., George, T., & Baliga, M. S. (2016). Chapter 50–ginger (*Zingiber officinale* Rosc.) oils A2 - Preedy. In R. Victor (Ed.), *Essential oils in food preservation, flavor and safety* (pp. 447–454). San Diego: Academic Press.
- Karaman, S., Yilmaz, M. T., Cankurt, H., Kayacier, A., & Sagdic, O. (2012). Linear creep and recovery analysis of ketchup–processed cheese mixtures using mechanical simulation models as a function of temperature and concentration. *Food Research International*, 48(2), 507–519.
- Kilara, A., & Vaghela, M. N. (2018). 4 - whey proteins. In *Proteins in food processing* (2nd ed., pp. 93–126). Cambridge: Woodhead Publishing.
- Lee, A. C., & Hong, Y. H. (2009). Coacervate formation of α -lactalbumin–chitosan and β -lactoglobulin–chitosan complexes. *Food Research International*, 42(5–6), 733–738.
- Liu, Y., Winter, H. H., & Perry, S. L. (2017). Linear viscoelasticity of complex coacervates. *Advances in Colloid and Interface Science*, 239, 46–60.
- Lu, G. W., & Gao, P. (2010). Chapter 3–emulsions and microemulsions for topical and transdermal drug delivery A2 - Kulkarni. In S. Vitthal (Ed.), *Handbook of non-invasive drug delivery systems* (pp. 59–94). Boston: William Andrew Publishing.
- Moschakis, T., Murray, B. S., & Biliaderis, C. G. (2010). Modifications in stability and structure of whey protein-coated o/w emulsions by interacting chitosan and gum Arabic mixed dispersions. *Food Hydrocolloids*, 24(1), 8–17.
- Muxika, A., Etxabide, A., Uranga, J., Guerrero, P., & de la Caba, K. (2017). Chitosan as a bioactive polymer: processing, properties

- and applications. *International Journal of Biological Macromolecules*, 105(Pt 2), 1358–1368.
- Ngo, D.-H., Vo, T. S., Ngo, D. N., Kang, K. H., Je, J. Y., Pham, H. N. D., Byun, H. G., & Kim, S. K. (2015). Biological effects of chitosan and its derivatives. *Food Hydrocolloids*, 51, 200–216.
- Retamal Marín, R. R., Babick, F., & Hillemann, L. (2017). Zeta potential measurements for non-spherical colloidal particles—practical issues of characterisation of interfacial properties of nanoparticles. *Colloids and Surfaces A: Physicochemical and Engineering Aspects*, 532, 516–521.
- Rocha, C. M., Souza, H. K., Magalhães, N. F., Andrade, C. T., & Gonçalves, M. P. (2014). Rheological and structural characterization of agar/whey proteins insoluble complexes. *Carbohydrate Polymers*, 110, 345–353.
- Rocha-Selmi, G. A., Theodoro, A. C., Thomazini, M., Bolini, H. M., & Favaro-Trindade, C. S. (2013). Double emulsion stage prior to complex coacervation process for microencapsulation of sweetener sucralose. *Journal of Food Engineering*, 119(1), 28–32.
- Rutz, J. K., Borges, C. D., Zambiazzi, R. C., Crizel-Cardozo, M. M., Kuck, L. S., & Noreña, C. P. (2017). Microencapsulation of palm oil by complex coacervation for application in food systems. *Food Chemistry*, 220, 59–66.
- Shi, Y., Li, C., Zhang, L., Huang, T., Ma, D., Tu, Z.-C., et al. (2017). Characterization and emulsifying properties of octenyl succinate anhydride modified Acacia seyal gum (gum Arabic). *Food Hydrocolloids*, 65, 10–16.
- Singh, G., Kapoor, I. P. S., Singh, P., de Heluani, C. S., de Lampasona, M. P., & Catalan, C. A. N. (2008). Chemistry, antioxidant and antimicrobial investigations on essential oil and oleoresins of *Zingiber officinale*. *Food and Chemical Toxicology*, 46(10), 3295–3302.
- Srinivasan, K. (2017). Ginger rhizomes (*Zingiber officinale*): a spice with multiple health beneficial potentials. *PharmaNutrition*, 5(1), 18–28.
- Stang, M., Karbstein, H., & Schubert, H. (1994). Adsorption kinetics of emulsifiers at oil–water interfaces and their effect on mechanical emulsification. *Chemical Engineering and Processing: Process Intensification*, 33(5), 307–311.
- Steffe, J. F. (1996). *Rheological methods in food process engineering* (2nd ed.). East Lansing: Freeman press.
- Stoyanova, A., Konakchiev, A., Damyanova, S., Stoilova, I., & Suu, P. T. (2006). Composition and antimicrobial activity of ginger essential oil from Vietnam. *Journal of Essential Oil Bearing Plants*, 9(1), 93–98.
- Tan, C., Xie, J., Zhang, X., Cai, J., & Xia, S. (2016). Polysaccharide-based nanoparticles by chitosan and gum arabic polyelectrolyte complexation as carriers for curcumin. *Food Hydrocolloids*, 57, 236–245.
- Tavares, L., & Noreña, C. P. Z. (2018). Encapsulation of garlic extract using complex coacervation with whey protein isolate and chitosan as wall materials followed by spray drying. *Food Hydrocolloids*, 89, 360–369.
- Timilsena, Y. P., Akanbi, T. O., Khalid, N., Adhikari, B., & Barrow, C. J. (2019). Complex coacervation: Principles, mechanisms and applications in microencapsulation. *International Journal of Biological Macromolecules*, 121, 1276–1286.
- Touré, A., Lu, H. B., Zhang, X., & Xueming, X. (2011). Microencapsulation of ginger oil in 18DE maltodextrin/whey protein isolate. *Journal of Herbs, Spices & Medicinal Plants*, 17(2), 183–195.
- Turgeon, S. L., & Laneuville, S. I. (2009). Protein + polysaccharide coacervates and complexes: from scientific background to their application as functional ingredients in food products. In S. Kasapis, I. T. Norton, & J. B. Ubbink (Eds.), *Modern biopolymer science* (pp. 327–363). San Diego: Academic Press.
- Ukeh, D. A., Birkett, M. A., Pickett, J. A., Bowman, A. S., & Jennifer Mordue, A. (2009). Repellent activity of alligator pepper, *Aframomum melegueta*, and ginger, *Zingiber officinale*, against the maize weevil, *Sitophilus zeamais*. *Phytochemistry*, 70(6), 751–758.
- Wang, Y., Xia, Y., Zhang, P., Ye, L., Wu, L., & He, S. (2017). Physical characterization and pork packaging application of chitosan films incorporated with combined essential oils of cinnamon and ginger. *Food and Bioprocess Technology*, 10(3), 503–511.
- Wee, M. S., Nurhazwani, S., Tan, K. W., Goh, K. K., Sims, I. M., & Matia-Merino, L. (2014). Complex coacervation of an arabinogalactan-protein extracted from the *Meryta sinclairii* tree (puka gum) and whey protein isolate. *Food Hydrocolloids*, 42, 130–138.
- Weinbreck, F., Wientjes, R. H., Nieuwenhuijse, H., Robijn, G. W., & de Kruif, C. G. (2004). Rheological properties of whey protein/gum Arabic coacervates. *Journal of Rheology*, 48(6), 1215–1228.
- Wu, D., Xu, J., Chen, Y., Yi, M., & Wang, Q. (2018). Gum Arabic: a promising candidate for the construction of physical hydrogels exhibiting highly stretchable, self-healing and tensility reinforcing performances. *Carbohydrate Polymers*, 181, 167–174.
- Ye, Q., Georges, N., & Selomulya, C. (2018). Microencapsulation of active ingredients in functional foods: from research stage to commercial food products. *Trends in Food Science & Technology*, 78, 167–179.
- Yilmaz, M. T., Karaman, S., Dogan, M., Yetim, H., & Kayacier, A. (2012). Characterization of O/W model system meat emulsions using shear creep and creep recovery tests based on mechanical simulation models and their correlation with texture profile analysis (TPA) parameters. *Journal of Food Engineering*, 108(2), 327–336.
- You, G., Liu, X. L., & Zhao, M. M. (2018). Preparation and characterization of hsian-tsoo gum and chitosan complex coacervates. *Food Hydrocolloids*, 74, 255–266.
- Zotarelli, M. F., da Silva, V. M., Durigon, A., Hubinger, M. D., & Laurindo, J. B. (2017). Production of mango powder by spray drying and cast-tape drying. *Powder Technology*, 305, 447–454.

Publisher's Note Springer Nature remains neutral with regard to jurisdictional claims in published maps and institutional affiliations.